ELSEVIER

Marine and Petroleum Geology 17 (2000) 199–218

Marine and Petroleum Geology

Influence of sea level and basin physiography on emplacement of the late Pleistocene Herodotus Basin Megaturbidite, SE Mediterranean Sea

Michael S. Reeder[a,*], R. Guy Rothwell[b], Dorrik A.V. Stow[a]

[a]*School of Ocean and Earth Sciences, University of Southampton, UK*
[b]*Challenger Division for Seafloor Processes, Southampton Oceanography Centre, European Way, Empress Dock, Southampton SO14 3ZH, UK*

Received 23 October 1998; received in revised form 13 August 1999; accepted 16 August 1999

Abstract

Radiocarbon ^{14}C dates from pelagic intervals above a megaturbidite in the Herodotus Basin give direct evidence of emplacement at the beginning of the last glacial period, approximately 27,125 calendar years before present, as sea level lowered rapidly and entered a low stand phase. The Herodotus Basin Megaturbidite is a basinwide deposit that forms a recognisable acoustically-transparent layer on 3.5 kHz high-resolution seismic profiles and covers an area of approximately 40,000 km^2. It thins from about 20 m in thickness proximally to some 10 m distally over a basin length in excess of 400 km. The total volume is estimated at around 400 km^3, which is significantly more than the volume of sediment that could have been displaced from its most likely source area, the funnel-shaped marginal embayment of the Gulf of Salûm to the west of the Nile Cone. The additional material may have been derived, in part, from synchronous failures on other parts of the Libyan/Egyptian shelf and slope, but most is believed to have come from large-scale erosion at the base of the very large-volume turbidity current that was generated from the original slide. Detailed sedimentary analyses of cores recovered from the megaturbidite show its distinctive characteristics: graded sand, silt, mud and bioturbated mud units; poorly developed structures proximally becoming more distinct and ordered distally; variation in grain size and structures that suggest either flow separation/reflection around topographic highs and/or an inherently unstable flow; and a mixed-source bioclastic-terrigenous composition. These features, together with its size and lateral extent, would make any similar megabed an excellent marker horizon in basin analysis. A combination of factors was responsible for triggering the initial slide-debris flow event that evolved downslope into this megaturbidity current. These include lowered sea level that destabilised the outer shelf — upper slope sediments, tectonic oversteepening of the margin, relatively high rates of sedimentation, and seismic activity.

Keywords: Herodotus Basin; Megaturbidite; Acoustically Transparent Layer; Low sea level; Physiography; Slope failure; Radiocarbon dating

1. Introduction

Megaturbidites are the deposits from large-volume turbidity currents, generated by large-scale slope failures and typically form stratigraphically extensive horizons in the geological record. They occur commonly in deep ocean basins having bypassed the feeder channels, fan or slope apron systems. Reports of megaturbidites have increased over the last decade since the term was introduced by Mutti, Ricci Lucchi, Seguret & Zanzucchi (1984) but little is known about their properties and the circumstances that govern the deposition of a large thickness and volume of sediment in one event. Megaturbidites can form a significant part of the basin fill and may be important as potential hydrocarbon reservoirs. Where they occur as basinwide deposits with distinctive characteristics, they are particularly important as stratigraphic markers.

* Corresponding author. Fax: +44-1420-22357.
E-mail address: mreeder@gaffney-chine.com (M.S. Reeder).

0264-8172/00/$ - see front matter
PII: S0264-8172(99)00048-3

The relationship between turbidite emplacement and eustatic sea level has been discussed in the literature (e.g., Shanmugam & Moiola, 1982, 1984; Vail, Mitchum Jr & Thompson III, 1977; Posamentier & Vail, 1988; amongst others). These reports suggest that turbidites in general are deposited preferentially during lowered sea level. The relationship between large-volume turbidity currents and sea level change has also been discussed by several authors but remains poorly understood (Weaver & Kuijpers, 1983; Cita et al., 1984a; Marjanac 1996; Rothwell, Thomson & Kahler, 1998). A review of the emplacement dates obtained from several reported case studies as well as the Herodotus Basin Megaturbidite discussed in this paper suggests that megaturbidites from the recent record (< 1 Ma BP) are generally related to sea level low stands whilst older deposits (> 1 Ma BP) have been ascribed predominantly to seismic events.

Several authors have attributed the emplacement of megabeds to seismic activity causing upslope slide failure, followed by its downslope evolution into a debris flow and turbidity current. Examples include recent deposits from the Sohm (Heezen & Ewing, 1952; Piper & Aksu, 1987) and Hatteras Abyssal Plains (Elmore, Pilkey, Cleary, Curran & Curran, 1979; Prince, Resing, Kulm & Moore Jr, 1974) and ancient examples such as the Gordo Megabed of the Tabernas Basin in SE Spain (Kleverlaan, 1987), the Doumsan Megabed in south Korea (Chough, Hwang & Choe, 1990), the Hecho Group Megabeds of the Spanish and French Pyrenees (Rupke, 1976; Labaume, Mutti, Seguret & Rosell, 1983; Seguret, Labaume & Madariaga, 1984; Puigdefabregas, 1986), and several examples from the northern Apennines (Bernouilli et al., 1981; Amorosi, Colalongo & Vaiani, 1996).

Other authors have proposed the influence of sea level on the initial triggering and subsequent emplacement of megaturbidites. Examples include the Horseshoe Abyssal Plain megaturbidites off the Iberian Margin (Lebreiro, McCave & Weaver, 1997), the Balearic Abyssal Plain Megabed of the western Mediterranean (Rothwell et al., 1998), the Madeira Abyssal Plain megaturbidites of the NW African Atlantic margin (Weaver & Rothwell, 1987; Weaver, Rothwell, Ebbing, Gunn & Hunter, 1992; Rothwell, Pearce & Weaver, 1992), submarine slumping of the southern margin of Israel, as well as Eocene examples from the Dalmatian flysch (Marjanac, 1996) and the Basco-Beanaise megabeds of the western Pyrenees (Souquet, Eschard & Lods, 1987).

The release of buried clathrates has also been proposed as a trigger mechanism for slides, in conjunction with sea-level change, seismic activity or thermal warming of sediments (Bugge, Befning, Belderson, Eidrun, Jansen, Kenyon et al., 1987, Evans, King, Kenyon, Brett & Wallis, 1996). Other mechanisms such as boloidal impacts (Iturralde-Vinent, 1992), tsunami wave impact (Cita, Camerlenghi, Kastens & McCoy, 1984b; Cita, Camerlenghi & Rimoli, 1996; Heike, 1984) and over-supply and under-consolidation of sedimentary material (Doyle & Bourrouilh, 1986) may be important factors in emplacement of some megabeds.

This paper describes the sedimentary and seismic characteristics of the late Pleistocene Herodotus Basin Megaturbidite (HBM) of the south-eastern Mediterranean Sea and details its relationship to eustatic sea level change and the physiography of the basin.

2. The Herodotus Basin

The Herodotus Basin forms the deepest part of the south-eastern Mediterranean Sea and is defined by the 3000 m isobath (Fig. 1). This elongate depression is bounded to the north-west by the accretionary prism complex of the Mediterranean Ridge (or Outer Hellenic Ridge) and to the south-east by the Nile Cone. The SW and NE ends of the basin are bounded by the Libyan/Egyptian continental slope and the Anatolian (or Florence) rise respectively. The deepest part of the basin (below the 3000 m isobath) has an approximate area of 40,000 km^2.

The evolution of the Herodotus Basin and the south-eastern Mediterranean region has been discussed by several authors (Stride, Belderson & Kenyon, 1977; Ross, Uchuoi, Summerhayes, Koelsch & El Shazly, 1978; Sestini 1984; Mart 1993, and others). Vertical migration of Messinian evaporites and compression associated with subduction of the African plate under the Eurasian plate deformed the northern boundary of the basin during the late Miocene and Pliocene (Mart, 1993). Progradation of the Nile Cone during the Pleistocene, folding, slumping and halokinesis on the Mediterranean Ridge accretionary prism and initiation of faulting of the coastal belt between Libya and the Nile Delta have all contributed to the present-day physical characteristics of the basin. The Nile Cone is encroaching northwards into the Herodotus Basin while the Mediterranean Ridge is accreting southwards narrowing the basin width and hence reducing its size over time (Reeder, Rothwell, Stow, Kahler & Kenyon, 1998). The oversteepened faulted continental slope and narrow shelf off North Africa led Sestini (1984) to describe the passive NE African margin as an "Unstable Shelf." The continental margin is characterised by late Miocene shallow-water marine carbonates and restricted-basin and sabkha evaporites, reflecting the dominance of marine rather than terrestrial sedimentation in the region (Sestini, 1984; Said, 1990).

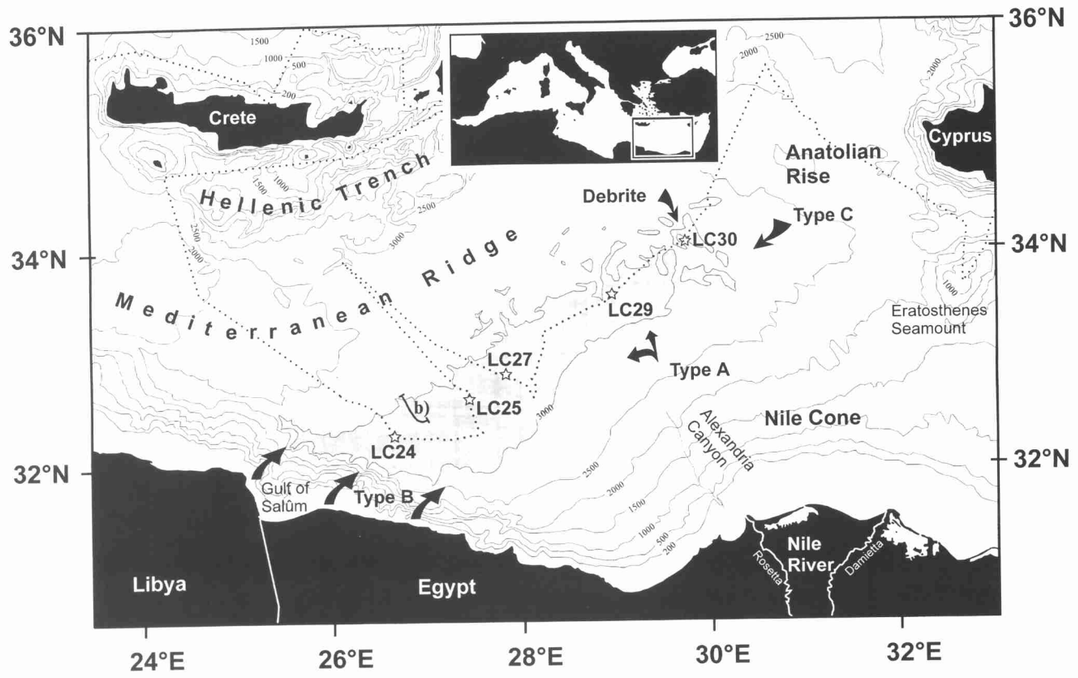

Fig. 1. Location map of the Herodotus Basin showing *Marion Dufresne* 81 track (dotted line), core positions, previous study transect '**b**' of Cita et al. (1984a) and Lucchi & Camerlenghi, (1993) and the four source input of allochthonous sediments during the late Pleistocene. Extent of turbidite basin is shown by shading.

2.1. Late Pleistocene Herodotus Basin sediments

The sediments of the Herodotus Basin are derived from four main sediment sources, and delivered to the basin by turbidity current and debris flow processes. Reeder et al. (1998) used the nomenclature of Cita et al. (1984a) to describe these sediment sources. Turbidites derived from the Nile Cone are termed 'Type-A,' and those derived from the Libyan/Egyptian Shelf termed 'Type-B.' A further source was identified by Reeder et al. (1998) and called 'Type-C' turbidites, being derived from the Anatolian Rise to the east of the basin. The fourth source is the Mediterranean Ridge along the northern flank of the basin from which localised debrites have been derived (Figs. 1 and 2).

The late Quaternary sediment sequence from the basin plain shows the majority of turbidites to be derived from the Nile Cone. These terrigenous quartz and organic-rich Nile Cone turbidites ('Type-A') are generally much thinner (15–750 cm thick) than the more calcareous Libyan/Egyptian shelf-derived ('Type-B') turbidites (6–1570 cm thick, see Fig. 2). Reeder et al. (1998) calculated an emplacement frequency of one turbidite approximately every 5 ka for the Nile Cone-derived turbidites and 1 per 6 ka for the Libyan/Egyptian source. The physical and mineralogical differences between the 'Type-A,' 'Type-B' and 'Type-C' turbidites are summarised in Table 1.

This paper differs from the previous studies of Reeder et al. (1998), Lucchi & Camerlenghi, (1993) and Cita et al. (1984a) by concentrating solely on the physical and sedimentological characteristics and the timing of emplacement of the HBM. It describes the detailed sedimentology and presents absolute radiocarbon dates of the megaturbidite, with inferences for the triggering and mode of emplacement. The general architecture, petrology and sedimentology have been described in the above previous studies and the reader is directed to these publications for a general overview of the late Pleistocene sedimentology and stratigraphy of the Herodotus Basin.

3. The Herodotus Basin Megaturbidite (HBM)

Five giant piston cores (Fig. 2) were recovered on a 350 km SW–NE transect of the Herodotus Basin during *Marion Dufresne* Cruise 81, with a spacing of

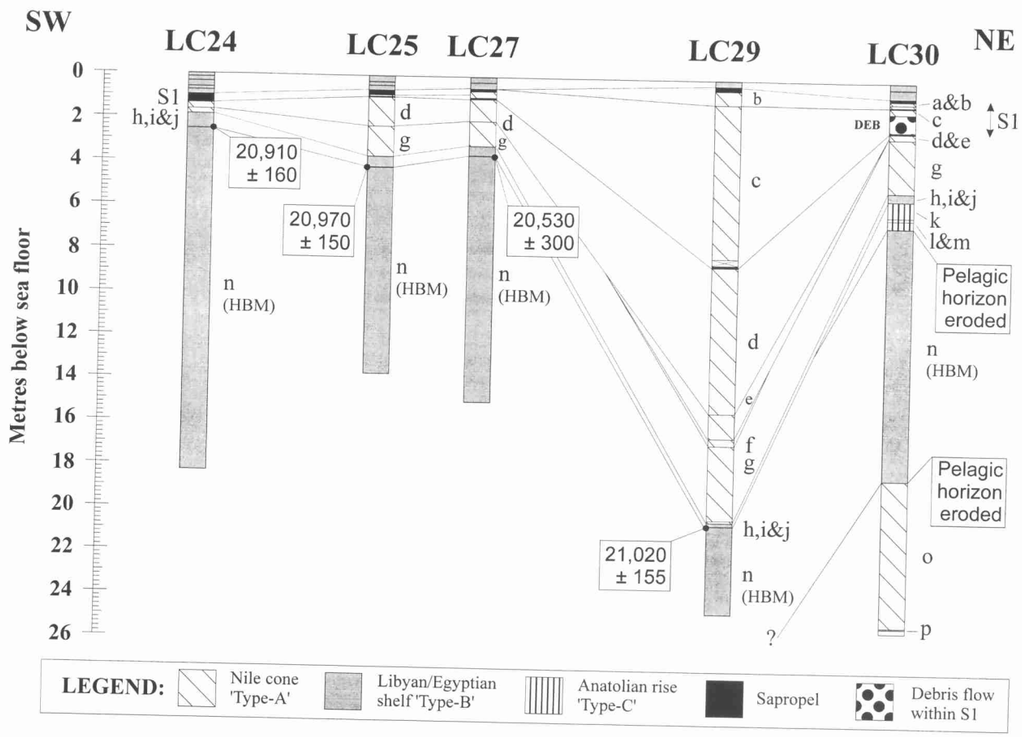

Fig. 2. Turbidite correlation in the five cores from the Herodotus Basin collected during *Marion Dufresne* cruise 81. The Herodotus Basin Megaturbidite (turbidite '*n*') dominates all five cores. Location of samples for radiocarbon dating are also shown.

50–100 km between core stations (Fig. 1 and Table 2). These cores are dominated by a >10 m thick, pale olive/grey mud unit showing a positively graded grain-size distribution and turbidite sedimentary structures. This thick unit has similar compositional and sedimentary and geochemical characteristics in each of the five cores, suggesting it was deposited from the same turbidity flow (Reeder et al., 1998).

High-resolution 3.5 kHz seismic profiles collected across the plain during the cruise show a thick, conspicuous, laterally-extensive acoustically transparent layer (ATL, Fig. 3). This layer is estimated to be 15–20 m in thickness and its upper boundary to vary between approximately 5–20 m below the seafloor (Fig. 3a and 3b). The relationship between this acoustically transparent layer (ATL) and the present day sea floor topography (Fig. 3c) is complex, but its estimated thickness and depth below the seafloor suggest that it corresponds to the thick mud megaturbidite identified in the five long-piston cores.

Table 1
Summary of the sedimentological differences between the 'Type-A' (Nile Cone), the 'Type-B' (Libyan/Egyptian shelf and upper slope) and the 'Type-C' (Anatolian Rise) turbidites

Characteristics	'Type A' turbidites	'Type B' turbidites	'Type C' turbidites
Colour	10YR3/2	10YR6/2	10YR6/4
Clay mineralogy	~80% Smectite	Equally proportionate Illite/Smectite	60% Smectite, 25% Illite
Thickness	15–750 cm	6–1570 cm	10–72 cm
Coarse fraction composition	Predominantly terrigenous	Mixed carbonate and terrigenous	Predominantly carbonate
Source	Nile Cone	Libyan/Egyptian slope and shelf	Anatolian Rise
Grain size	Mud and silty-mud	Silty and sandy muds	Mud with thin silty bases
Sedimentary structures	Few laminae	Abundant laminations	None
Calcium carbonate percentage	~10%	>40%	~40%
Number if events during period of study (~28 ka)	8	4	3

Table 2
Location of the Herodotus Basin long-piston cores collected during *Marion Dufresne Cruise 81 (Cruise report, Rothwell 1996)*

Core	Latitude	Longitude	Water depth (corrected m)	Core length (m)
LC24	32°17.71′N	26°37.95′E	3191	18.31
LC25	32°36.01′N	27°23.25′E	3129	13.71
LC27	32°48.91′N	27°40.45′E	3131	14.95
LC29	33°35.63′N	28°56.32′E	3138	24.66
LC30	34°04.70′N	29°42.72′E	3144	25.82

4. Analytical methods

To determine the sedimentological and physical properties of the HBM, post-cruise study of the Herodotus Basin cores included standard sedimentological visual description and sampling for grain size, calcium carbonate content ($CaCO_3$%), geochemical analysis by inductively coupled plasma atomic emission spectroscopy (ICP-AES) and micropalaeontological analysis of foraminifera and nannofossils for dating purposes. The results for the complete stratigraphy recovered from the Herodotus Basin are published elsewhere (Reeder et al., 1998).

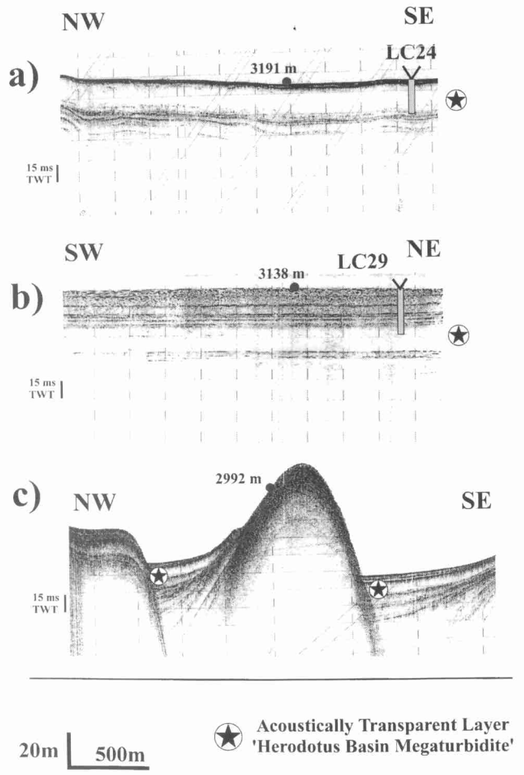

Fig. 3. The 'Acoustically Transparent Layer' — believed to be the seismic expression of the HBM as seen in 3.5 kHz high-resolution seismic profiles (a) approaching core station LC24, (b) approaching station LC29 and (c) presence between deformation ridges near LC25. Core site LC29 marks the present day depocentre on the plain. Note the difference in depth of the ATL at the different sites and how that relates to the observed depth of the HBM in the core descriptions, Fig. 2.

4.1. Grain size analysis

Grain size analyses of the HBM were made on 59 sediment samples taken from core LC30, with a sample spacing between 4 and 50 cm. Spacing was greater in the mud unit and closer in the basal silts and sands. Each sample was wet sieved to separate the sand (>63 μm) and mud fractions. The fine fraction (<63 μm) was then dried, re-suspended in 0.1% Calgon solution and analysed using a Micromeritics 5100 sedigraph.

4.2. Calcium carbonate content

Calcium carbonate ($CaCO_3$) content was determined by acid treatment of hand-ground sediment and coulometric detection of CO_2. Between 12 and 25 samples were collected for analysis of the HBM from each of the five cores.

4.3. Geochemical analysis

Geochemical analysis of 22 major, minor and trace elements from the Herodotus Basin turbidites aided correlation of units between cores. The analyses were performed using ICP-AES after digestion of 0.5 g of sample with a combination of hydrofluoric, perchloric and nitric acids had taken place. Precision was better than 5% for all elements and standard reference materials and in-house standards were used to monitor analytical accuracy. The results were first normalised to their Al_2O_3 value, and then scaled using Grant's (1986) Isocon Diagram method to facilitate correlation (see Reeder et al., 1998).

4.4. X-ray diffraction analysis

X-ray diffraction analysis of four samples from each of the proximal (LC24) and distal (LC30) HBM measured bulk-mineral and clay-mineral composition from the bioturbated mud top, the homogeneous mud, the silt and the sand units. Bulk-mineral analysis was achieved by drying 0.5 g of sample and grinding it to a fine powder. Clay mineral analyses were run following treatment with 10% acetic acid to remove carbonate material, followed by the addition of 1% Calgon solution to suspend the fine-sediment fraction. Centrifugal removal of the >2 μm fraction, the addition of 10% $MgCl_2$ solution and further centrifugal mechanical settling allowed the separation of the <2 μm clay fraction. The <2 μm samples were smeared on glass slides and dried to air temperature, 375°C, 550°C and glycolated at 55°C. All samples were analysed on a Philips PW1730 X-ray diffractometer.

4.5. AMS ^{14}C dating

This has been used to date the HBM following the method of Thomson and Weaver (1994), which overcomes the inherent problem of inclusion of older material during the emplacement process by sampling the pelagic horizons rather than the turbidite directly. Ideally, the method includes sampling planktonic foraminifera from pelagic horizons directly overlying and underlying the megaturbidite thereby bracketing emplacement times. However, even though the base of the megaturbidite was cored in LC30 there were no underlying pelagic sediments. This may be due to the megaturbidite eroding into an underlying Nile Cone derived turbidite ('o') removing any dateable pelagic horizon (LC30, Fig. 2). Therefore, only minimum emplacement dates could be obtained for the megaturbidite. These minimum dates will have a greater or lesser standard deviation depending on the thickness of the pelagic interval. However, time resolution cannot be improved by simply sampling a thinner portion of the pelagic layer because of bioturbation by benthic fauna.

Larger planktonic foraminifera are expected to be the least susceptible component of the pelagic interval to be redistributed by currents and thus the most suitable for dating. Sieving of the pelagic and turbidite mud obtained the >150 μm size fraction and only the clean planktonic foraminifera and pteropods were selected.

5. Sediments and sedimentary structures of the HBM

The HBM can be subdivided into four main sedimentary units that are readily distinguished on the basis of colour, sedimentary structures and grain size. They comprise: (1) a basal *sand unit*, which is generally structureless and medium yellowish brown in colour (10YR5/2); (2) a *silt unit*, which is laminated or cross laminated and light to medium olive grey in colour (5Y5/1 dark laminae, 5YR7/1 pale laminae); (3) a *mud unit*, the thickest of the four, normally graded from silty mud to clayey mud and moderate olive grey in colour (5Y4/2); and (4) an uppermost, paler, light olive grey-coloured *bioturbated mud unit* (5Y5/2). Colours and descriptions are based on the Munsell colour scheme (USGS Rock Color Chart Committee, 1991).

The complete HBM was only penetrated at the most distal site (LC30, Fig. 2) where its thickness is measured at 11.68 m. At this site, the sand unit accounts for only 0.5% of the total thickness, the silt unit 12%, the mud unit 85% and the bioturbated mud unit 2.5%. Based on 3.5 kHz profile data we can estimate the proximal thickness of the HBM at 18–20 m (LC24). Assuming the larger value, the sand unit has increased to 26% of the total, at the expense of the silt (5%) and the mud units (67%) (Table 3).

5.1. Sedimentary petrology

Petrographic analysis of smear slides and grain mounts of the bulk sediment and coarse-grained basal sand unit (>63 μm) respectively shows an approximate composition for the HBM of quartz (30%), unspecified calcite grains (15%) and a high proportion

Table 3
Thickness of the sedimentary units of the HBM in cores LC24 to LC30. Unit thickness percentages of the megaturbidite in core LC24 are calculated as a proportion of 20 m, estimated from 3.5 kHz high-resolution seismic profiles (Fig. 3)

Megaturbidite divisions	Thickness in cm (percent of total thickness)				
	LC24	LC25	LC27	LC29	LC30
Megaturbidite (total)	> 1626 (est. 20 m)	> 952	> 1133	> 410	1168
Bioturbated mud unit	46 (2.3%)	44	53	29	27 (2.3%)
Mud unit	1337 (66.9%)	734	772	> 381	997 (85.3%)
Silt unit	94 (4.7%)	72	60	X	139 (11.9%)
Sand unit	> 149 (26.1%)	> 102	> 248	X	5 (<0.5%)

of shelf derived bioclastic material (45%). The bioclastic material includes fragments of gastropods, sponge spicules, bivalves, bryozoans, pteropods, echinoid spines, and shallow-water benthic and planktonic foraminifera. Minor amounts of muscovite mica, translucent white and grey pumice grains, dark ferromagnesian minerals (e.g. pyroxenes and amphiboles) and a few cuspate and lunate mafic volcanic glass shards are also present. Previous studies of the HBM by Lucchi and Camerlenghi, (1993) and Cita et al. (1984a) detailed the clay mineralogy of the turbidite mud as well as the composition and grain size of the sand fraction. From these results the authors determined that the HBM was sourced from the carbonate shelf and upper slope of the NE African Margin to the west of the Nile Delta.

5.2. Grain size analysis

5.2.1. Mean size

Detailed analysis through the complete HBM in the most distal core (LC30) shows normal grading from sandy coarse silt to fine silty clay (Fig. 4a). The lower two units show the most marked grading from a basal mean grain size of 81 μm to around 7 μm at the top of the silt unit. There is also a distinct grain size fluctuation of about 20 μm in the basal units (sampling interval 4 cm), that becomes less evident in the silt unit. The thick mud unit shows an overall gradation from a mean size of 6–7 μm at the base to 2–4 μm at the top. There is a rather irregular fluctuation within these limits, both in terms of grain size grade and peak spacing, at least part of which we believe is of primary hydrodynamic origin rather than due to analytical error. The topmost bioturbated unit is the finest, with a mean grain size of 2–3 μm.

5.2.2. Size distribution

Grain size distribution is illustrated by selected samples from each of the HBM units (Fig. 4b). Sample 4, from near the base of the sand unit, is well sorted with a pronounced mode at 70 μm and a slight positive skewness. Sample 3, from the middle of the silt unit, is more poorly sorted with a primary mode at 16

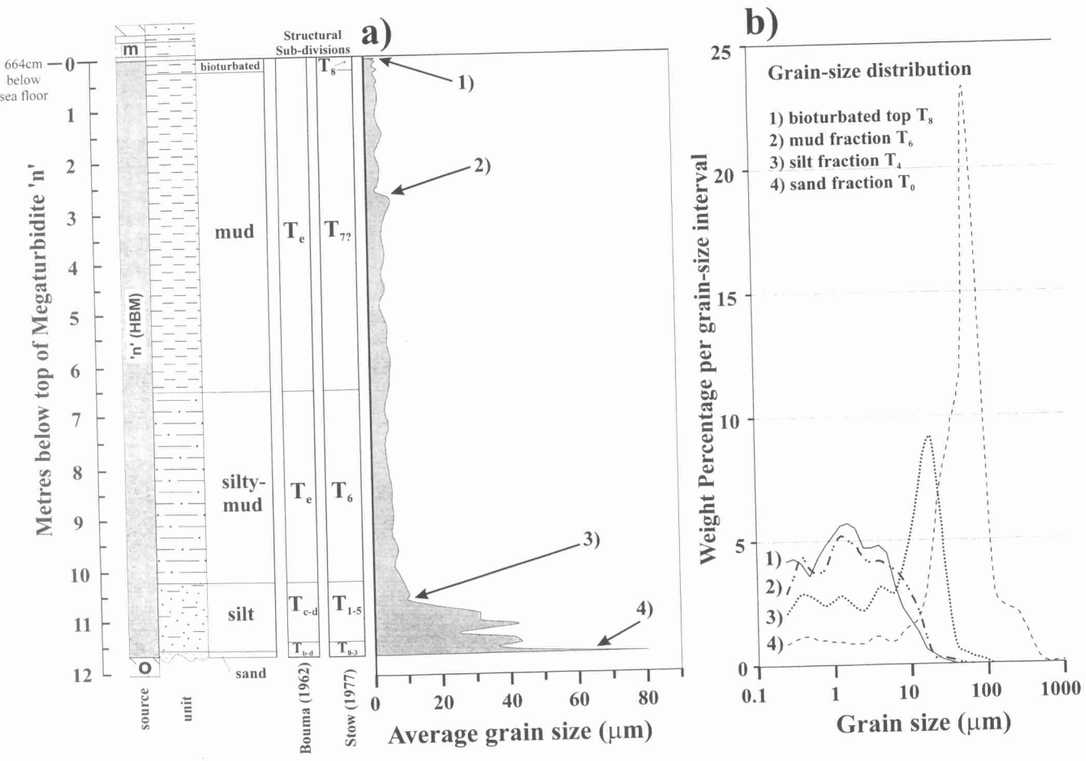

Fig. 4. Grain size analysis of the HBM. (a) Average grain size of the HBM in core LC30 (the most north-easterly and distal core from source). (b) Grain-size distribution curves for the bioturbated top, mud, silt and sand intervals of the HBM. Structural divisions after Bouma (1962) and Stow (1977).

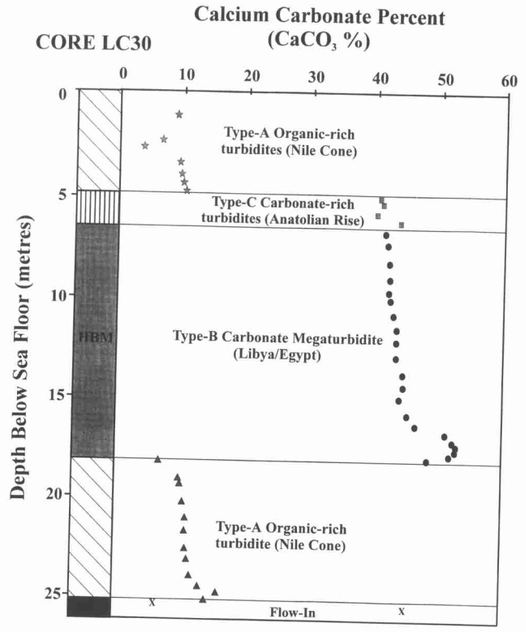

Fig. 5. Downcore calcium carbonate percentage in core LC30. Note the relatively high carbonate percentages in the turbidites derived from the North African shelf and Anatolian Rise compared to those from the Nile Cone.

μm (medium silt), three secondary modes within the finer tail, and a strong positive skew. Samples 2 and 1, from the mud and bioturbated mud units respectively, are both polymodal, poorly sorted and very fine grained. Poorly defined modal values occur at <1 μm, 1–2 μm and 3–4 μm.

Table 4
Bulk XRD mineralogy for the four structural units of the Herodotus Basin Megaturbidite, both proximally (LC24) and distally (LC30)

Turbidite/unit/source	Calcite %	Quartz %	Mica %	Dolomite %	Halite %	Feldspar %	Other %
Herodotus Basin Megaturbidite							
LC24 bioturbated mud	69	13	10	8	0	0	
LC24 mud	74	10	8	8	0	0	0
LC24 silt	56	12	6	11	8	0	0
LC24 sand	46	37	0	8	6	0	8 (rutile)
LC30 bioturbated mud	64	13	8	7	6	0	3 (rutile)
LC30 mud	62	15	8	8	8	0	0
LC30 silt	48	37	3	10	3	0	0
LC30 sand	40	46	3	7	4	0	0
Nile Cone[a] 'Type-A'	25	31	14	0	12	14	0
Libyan/Egyptian slope[a] 'Type-B'	50	23	5	10	7	5	4 (gypsum)
Anatolian Rise[a] 'Type-C'	53	16	8	9	7	7	0

[a] Average bulk mineralogy of turbidites from the three recognised sources (from Reeder et al., in prep.).

5.3. Geochemical analyses

5.3.1. Calcium carbonate percentage

The $CaCO_3$ percentage ranges from about 40% in the fine-grained muds of the distal region (LC30) to just less than 65% in the coarse sand fraction of the proximal region (LC24) (Fig. 5). The maximum value is found in the basal sands of the turbidite probably reflecting the greater abundance of larger bioclastic grains in the basal sand. Cita et al. (1984a) measured $CaCO_3$ percentages of just less than 85% in the basal sands. Towards the top of the megaturbidite, the mud and bioturbated-mud units commonly have calcium carbonate percentages of 40–50% and an almost equal amount of terrigenous material.

5.3.2. X-ray diffraction

The analysis of eight samples from the HBM shows that the mineralogy of the unit varies with both transport distance and between the different sedimentary units (Table 4). The bulk mineral analysis shows that quartz accounts for between 10–15% of the bioturbated and homogeneous mud units and increases to approximately 45% in the parallel laminated silts and cross laminated sands. The clay mineral assemblage is dominated by smectite (69%), with 17% illite and subordinate kaolinite (9%) and chlorite (5%). These proportions remain relatively constant throughout the length of the megaturbidite and can be readily distinguished from turbidites sourced from other regions (Table 5). The HBM has a mixed clay composition and can not be described simply as a being a 'Type-A' Nile Cone-derived turbidite nor a 'Type-B' Libyan/Egyptian shelf-derived turbidite but, rather, as a combination of the two. This may be due to the erosion and incorporation of underlying Nile Cone-derived material by the Libyan/Egyptian shelf-derived HBM turbidity current.

Table 5
Clay mineralogy for the four structural units of the Herodotus Basin Megaturbidite, both proximally (LC24) and distally (LC30). The clay mineralogy of the HBM may be interpreted as a 'mixture' of the 'Type-A' and 'Type-B' turbidites

Turbidite/unit/source	Smectite %	Illite %	Kaolinite %	Chlorite %
HBM	68	19	8	5
LC24 bioturbated mud unit	65	20	10	5
LC24 mud unit	70	16	9	5
LC24 silt unit	62	22	10	6
LC24 sand unit	67	17	9	7
LC30 bioturbated mud unit	70	15	9	6
LC30 mud unit	73	15	8	4
LC30 silt unit	74	14	7	5
LC30 sand unit	69	17	9	5
Average				
Nile Cone[a] 'Type-A'	83	7	6	4
African Shelf/Slope[a] 'Type-B'	44	40	9	7
Anatolian Rise[a] 'Type-C'	61	25	8	6

[a] Average clay mineralogy of turbidites from the three recognised sources (from Reeder et al., in prep.).

5.3.3. ICP-AES geochemical analysis

Each turbidite has a unique geochemical signature (Reeder et al., 1998) and can be correlated across the basin using chemostratigraphy (Pearce & Jarvis, 1995). Although the colour and petrology of the HBM are clearly different from those of the Nile Cone- and Anatolian Rise-derived turbidites, geochemical fingerprinting further confirms the correlation of individual beds between the five basin plain cores (Fig. 6).

5.4. Sedimentary structures

Sedimentary structures and thickness of the megaturbidite vary along the length of the basin from proximal (LC24) to distal (LC30) regions (Table 3). Structural divisions are recognised that can be related to turbidite divisions of the Bouma (Ta-Te) (Bouma, 1962) and Stow (T0-T8) (Stow, 1977) models. In cores LC24 to LC29, there is an indistinct parallel-lamination and lensing in the part of the lower sand/silt units penetrated but no other sedimentary structures are present. Lucchi and Camerlenghi, (1993) described the basal sands and silts as having 'neither parallel or convolute lamination present'. However, in core LC30 the HBM has recognisable sedimentary structures which may be described in terms of either the Stow (1977) fine-grained or the Bouma (1962) medium-grained turbidite facies models (Figs. 4 and 7). The HBM can be subdivided into a number of structural units, based on these facies models.

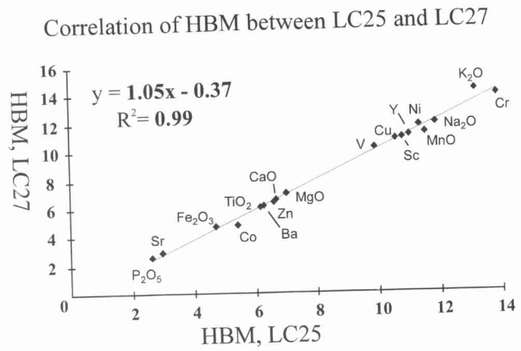

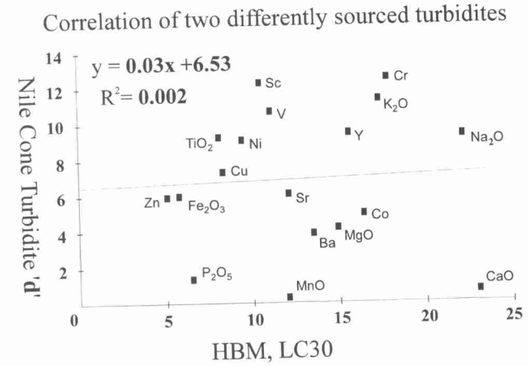

Fig. 6. Two examples of the chemostratigraphic technique used for correlating the Herodotus Basin turbidites. (a) Excellent correlation seen when samples of the HBM mud fraction are analysed from two different cores, LC25 and LC27, approximately 50 km apart. (b) Poor correlation seen when a Nile Cone-derived turbidite and the HBM demonstrating the marked compositional differences between the two beds.

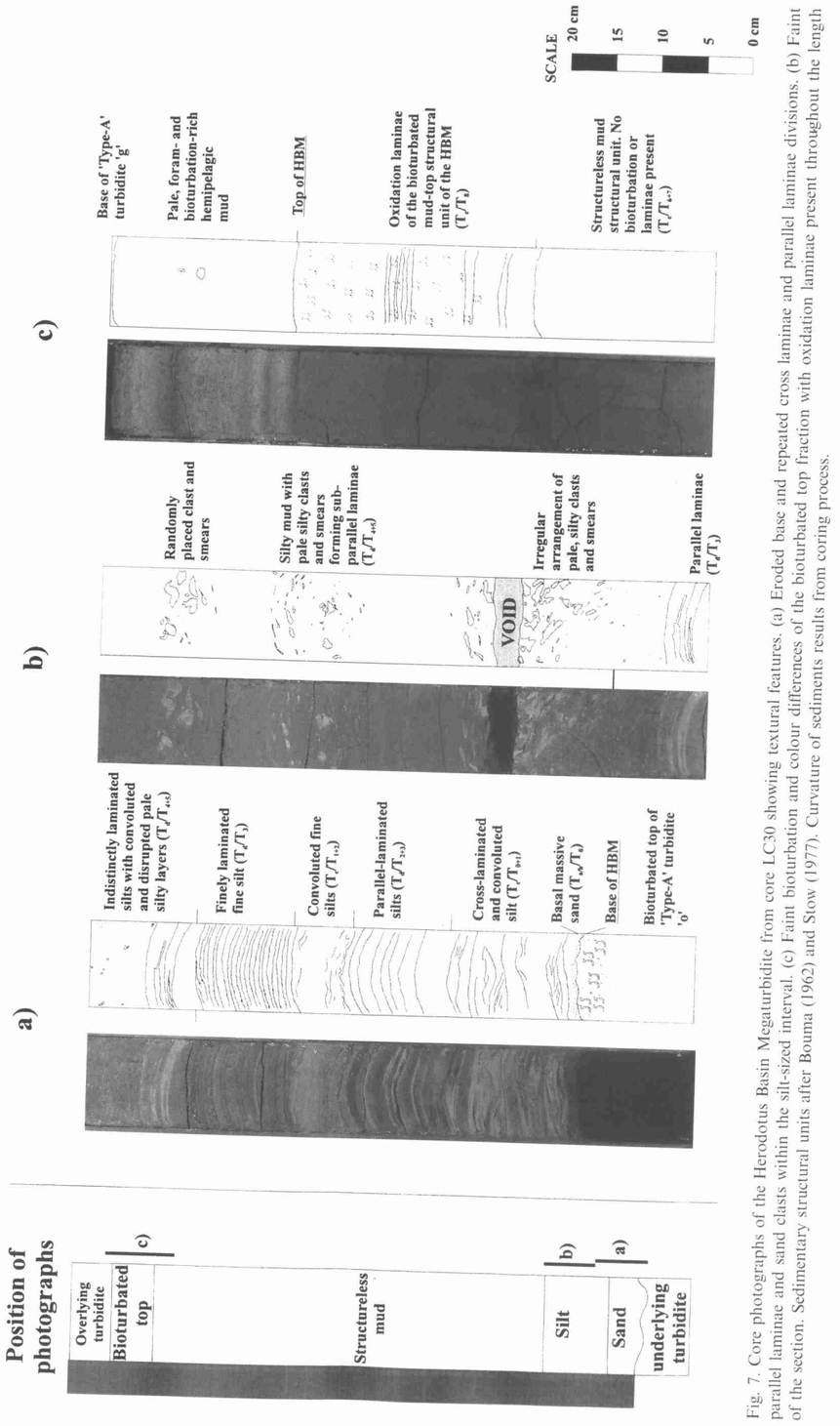

Fig. 7. Core photographs of the Herodotus Basin Megaturbidite from core LC30 showing textural features. (a) Eroded base and repeated cross laminae and parallel laminae divisions. (b) Faint parallel laminae and sand clasts within the silt-sized interval. (c) Faint bioturbation and colour differences of the bioturbated top fraction with oxidation laminae present throughout the length of the section. Sedimentary structural units after Bouma (1962) and Stow (1977). Curvature of sediments results from coring process.

5.4.1. Massive basal sand (Bouma Ta/b or Stow T0)

In core LC30 a 2 cm thick coarse sand containing bioclastic material has eroded into the underlying strata. It is difficult to determine whether the sand is massive or laminated and it is therefore denoted Ta/B. The unit could be considered equivalent to the Stow structural division T0 (basal lenticular silt lamina). At this distal location it seems unlikely that more than a few centimetres of the underlying turbidite has been removed as 10 cm of the bioturbated mud top of Nile Cone-derived turbidite 'o' is present (Fig. 7a). However, in the more proximal regions Lucchi and Camerlenghi (1993) noted that the megaturbidite truncates a 'Type-B' turbidite (Libyan/Egyptian-derived) on the lower slopes of the Mediterranean Ridge (core 12) but erodes into a 'Type-A' turbidite (Nile Cone-derived) just 5 km further north (location in Fig. 8). We cannot estimate the amount of basal erosion that has taken place in this area.

5.4.2. Convoluted/cross-laminated silt (Bouma Tc or Stow T0/1)

The thin basal sand passes directly into a 14 cm thick cross-laminated and convolute sand/silt with laminae picked out by a darker mineral assemblage (predominantly dark igneous minerals). The cross lamination tends to show a uni-directional flow with laminae truncated in only one direction (Fig. 7), although the unit is quite convolute and shows some coring disturbance so that we cannot rule out the possibility of flow reflection and/or pulsing. This 14 cm thick unit equates to an expanded T0/T1 Stow division (rippled and convolute silt laminae).

5.4.3. Parallel laminated silts (Bouma Td or Stow T2+3)

The section passes upward into an 11 cm thick sub-parallel laminated fine sand/silt. The interpretation of this as representing Stow divisions T2 (irregular, thin lenticular silt laminae) and a thicker T3 (regular parallel silt laminae) would suggest that it equates to the Bouma division Td, rather than a repetition of Tb.

5.4.4. Convoluted and irregular laminated fine silts (Bouma Tc or Stow T1+2)

The standard sequence becomes disordered upwards,

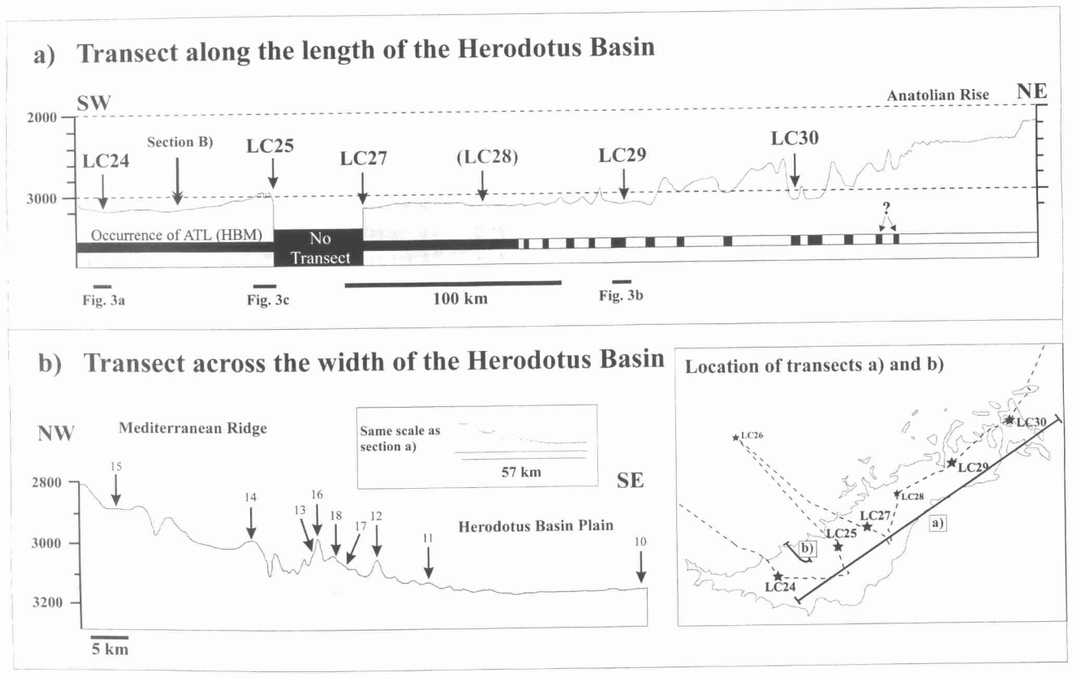

Fig. 8. Bathymetric cross sections of the Herodotus Basin. (a) Along the length of the basin showing the distribution of the HBM from 3.5 kHz seismic profiles (corrected m). Note the increased deformation to the NE (Anatolian Rise). The occurrence of the ATL seen in Fig. 3, is marked in black beneath the bathymetry. (b) Across the width of the basin between core sites LC24 and LC25 ('b') showing the increased deformation towards the NW (Mediterranean Ridge). Section and core locations from Cita et al. (1984a) are shown. Both sections are at 40:1 vertical exaggeration with (b) at a larger scale.

first with a repetition (7 cm) of the Tc convolute laminated silt seen 11 cm below. The laminae are fairly pervasive throughout the core section resembling a finer-grained version of the Stow T1 and T2 divisions. The wavy laminae are here considered to be too distinct to be the wispy silt laminae of Stow division T5.

5.4.5. Finely laminated silts (Bouma Td or Stow T3)

There is further repetition of the standard sedimentary structural divisions with the reappearance of a 13 cm thick millimetric parallel laminated fine silt. The laminae are both uniform through the section and pervasive across the 10 cm diameter of the core but are clearly finer-grained than the 11 cm thick Td/T3 structural unit below.

5.4.6. Indistinctly laminated silts (Bouma Td or Stow T4+5)

The silt unit is mostly characterised by faint millimetric-scale parallel laminae, equivalent to Bouma Td or Stow's T4 division. In the distal location, the fine-grained indistinctly-laminated silts are separated by a number of slightly coarser-grained silt horizons (3–6 cm thick), that show intense convolution and disruption (Fig. 7). These horizons display features similar to those of very rapidly deposited turbidite silty muds found in a proximal levee location (e.g. on the Mississippi Fan, Stow et al., 1985).

5.4.7. Structureless muds (Bouma Te or Stow T6+7)

The mud unit is completely structureless, although cyclic variation in grain-size together with slight overall upward fining is revealed by detailed grain-size analysis (see Section 8). This unit shows the sedimentary characteristics of the Bouma turbidite division Te or Stow division T6 and T7 (graded and ungraded turbidite muds respectively). This structural division is proportionally the thickest unit of the HBM in the cores, although the presumed maximum thickness of the sand unit could not be determined because of incomplete penetration of the turbidite in more proximal cores LC24 to LC29.

5.4.8. Bioturbated/oxidised top (Bouma Te or Stow T8)

At the very top of the mud unit is a 27 cm thick mud interval which is distinctly lighter in colour than the main body of the HBM. The unit is moderately bioturbated for most of its thickness, with bioturbation increasing up-section (Fig. 7). Recognisable burrows include mainly *Chondrites* and possibly *Planolites* and oxidation of the sediments has left some bands of coloration which are thought to be successive post-depositional oxidation fronts rather than primary parallel laminae (Thomson, Higgs, Croudace, Colley & Hydes, 1993). Little or no erosion caused by successive events is seen at the top of the bioturbated megaturbidite unit as the pelagic/hemipelagic horizon is present above the HBM. The bioturbated top most probably equates to Stow structural division T8, although its very thick development in some cores (up to 53 cm) and its very fine grain size make it similar to the hemiturbidites described from the distal Bengal Fan (Stow & Wetzel, 1990).

6. Geometry of the HBM

The HBM is only fully penetrated in the distal core location (LC30), where it has a thickness of 11.68 m (Fig. 2). Proximally, (LC24–LC27), the megaturbidite is only penetrated to the coarse sand unit to a maximum total thickness of 16.26 m. The HBM can be traced on the 3.5 kHz profiles as an acoustically transparent layer along the length of the Herodotus Basin for a distance of approximately 400 km, although it is expected that the megaturbidite may be present further to the NE than noted in the cores or the seismic survey. Estimates from the 3.5 kHz high-resolution seismic profiles show that the HBM is approximately 20 m thick in the proximal locations and decreases to around 8–10 m thick distally.

Across the width of the Herodotus Basin (SE–NW) the HBM can be traced over a distance of about 100 km, the thickness varying with the basin floor topography (Fig. 3c, Table 6). It is seen to pinchout onto the Mediterranean Ridge as well as against within-basin topographic highs. Continued deformation and associated ridge uplift are seen to drag up the basinal sediments, including the HBM, some 30–40 m above the basin floor.

Just as the total thickness of the HBM is influenced by topography, so the thickness of individual sedimentary units varies. Cita et al. (1984a) and Lucchi & Camerlenghi, (1993) showed that the distribution and proportion of the textural intervals of the megaturbidite vary from core to core, depending on the location of the cores on ridges and troughs. Reduced thicknesses (< 1 cm) of the megaturbidite are found on the topographic highs but these thin veneers of the HBM comprise almost 100% sand.

The volume of the HBM can be estimated from the occurrence of the acoustically transparent layer and the average thickness of the megaturbidite (Fig. 8). Previous studies by Cita et al. (1984a) and Lucchi & Camerlenghi (1993) estimated a conservative volume of 10 km^3 from their transect across the width of the basin, assuming lateral supply and restricted extent along the basin axis. However, Reeder et al. (1998)

and this study have shown the much greater basinwide extent and hence recalculated the volume of megaturbidite '*n*' to be much larger at approximately 400 km^3. This figure is based on the area of the basin at the 3000 m isobath being approximately 40,000 km^2 and that the average thickness of the megaturbidite being approximately 10 m.

7. Dating of emplacement of the HBM

Using the high-resolution nannofossil zonal scheme of Weaver (1983), the pelagic layers above the megaturbidite were biostratigraphically dated and found to fall within Weaver Zone 1 (dated by calibration with Pleistocene oxygen isotope stages). Dominance of *Emiliania huxleyi* in the samples showed that the emplacement of the HBM was no earlier than 60 ka (Kahler & Dossi, 1996). Reeder et al. (1998) estimated the date of deposition at 27.5 ka before present by summing the thicknesses of pelagic horizons above the HBM and dividing by an estimated pelagic accumulation rate of 2–3 cm/ka, reported as a typical rate for the eastern Mediterranean (E. Rohling, personal communication).

Four radiocarbon dates were obtained by AMS dating of material from pelagic/turbidite horizons at the top of the HBM in cores LC24, 25, 27 and 29 (Fig. 2, Table 6). These dates range between 20,530 and 21,020 radiocarbon years (average 20,860). The correction of Bard, Arnold, Fairbanks & Hamelin (1993) was made to account for the relationship between the radiocarbon and calendar timescales. The relationship is given as 'Calendar Years = 1.24(^{14}C years)−440'. This includes a correction of 400 years to account for the offset ^{14}C age of the atmospheric and oceanic mixed-layer reservoir (Stuiver, 1990). The value for the average calendar date of the overlying pelagic layers, and hence the minimum emplacement date (HBMmin) is 25,425 years before present.

To obtain a maximum and consequent average date for the HBM emplacement a comparison was made with radiocarbon dates found by Rothwell et al. (1998). Study of a similar-sized megabed from the Balearic Abyssal Plain in the western Mediterranean, which was deposited at a similar date, has shown that the average difference between the dates of the pelagic sediments above and directly below the megaturbidite is approximately 3400 calendar years (cf Rothwell et al., 1998). This difference may be due to the erosive process of the megaturbidite emplacement, consequently increasing the dates obtained for the underlying pelagic intervals. Applying the same differential to the HBM yields maximum and average calendar dates of HBMmax 28,825 and HBMave 27,125 years BP, respectively.

Table 6
Radiocarbon and calendar ages for pelagic intervals overlying the Herodotus Basin megaturbidite

Core	Depth below seafloor (m)	δ^{13}C value	δ^{18}O value	Lab. sample number	Radio-carbon dates (^{14}C Years)		Calendar years before present[a]		
					Minimum age	error ($\pm 1\sigma$)	Minimum age	Maximum age[b]	Interpolated depositional age
LC24	2.23–2.37	1.5	3.7	AA-24170	20,910	160	25,490	28,890	27,190
LC25	4.16–4.29	1.4	3.1	AA-24166	20,970	150	25,565	28,965	27,265
LC27	3.61–3.76	1.5	3.4	AA-24167	20,530	300	25,015	28,415	26,715
LC29	20.54–20.67	−1.5	N/A	AA-24165	21,020	155	25,625	29,025	27,325
				Average	20,860	190	HBMmin 25,425	HBMmax 28,825	HBMave 27,125

[a] Equation calendar year is 1.24(^{14}C yr) −440 yr to convert Conventional ^{14}C ages to calendar years BP, (Bard et al., 1993).
[b] +3400 year correction interpolated from ^{14}C dates of horizons above and below megaturbidite of Rothwell et al. (1998).

8. Discussion

8.1. Source and volume

Previous work by Lucchi and Camerlenghi (1993) and Cita et al. (1984a) indicates that the most likely source of the Herodotus Basin Megaturbidite is the Libyan/Egyptian continental shelf to the west of the Nile Cone, due to its clear compositional affinity to turbidites sourced from this region. Their clay mineralogy varies considerably to the results presented in this paper. The HBM has a mixed composition, which does not have an affinity with any of the three sources. The terrigenous part of the bulk mineralogy may be from erosion of underlying Nile Cone turbidites and the clay mineralogy from the supply of terrigenous-derived clays from the Hellenic Arc islands, transported by the anti-cyclonic eastern Mediterranean gyre (Cita et al., 1984a).

Cita et al. (1984a) calculated a volume of only 10 km^3 for the HBM and suggested that the sediment pathways were two or more small canyons leading from the shelf to the slope. This study, using the revised volume of 400 km^3, suggests removal of a larger amount of sediment, which possibly resulted in a slide and maybe a slide scar. The Gulf of Salûm, in the extreme south-western end of the Herodotus Basin, may be a possible source where a large semi-circular 'funnel-shaped' embayment is seen in the present day bathymetry (Fig. 9). Volumetric calculations of the turbidite and the possible amount of material removed to form the Gulf of Salûm, using the bathymetry of the GEBCO Digital Atlas (Jones, Tabor & Weatherall, 1994), correlate moderately well. The amount of sediment estimated to have been removed is approximately 300 km^3. The additional estimated 100 km^3 may have come from the synchronous collapse on the smaller canyons as suggested by Cita et al. (1984a) and/or from erosion at the base and margins of the giant turbidity current.

Collapse of the shelf and upper slope in the faulted Gulf of Salûm region might be expected to have created a slide scar if the downslope movement evolved from a slide to a debris flow and finally a turbidity current. However, the bathymetry shows no evidence of a slide scar, which may suggest either that there have been more recent collapses masking the earlier scarp, or that the slide was on a planar, low-angle detachment, such as weak strata in the sedimentary sequence. Both of these factors are possible as other Libyan/Egyptian continental margin-derived turbidites are present in the Herodotus Basin (turbidites h, i and j, Fig. 2) and there are weak strata, such as the Messinian evaporites (~6 Ma), in the sedimentological record. The Messinian evaporites are reported as having been precipitated along the Libyan/Egyptian continental margin in high-salinity nearshore lagoons or semi-enclosed gulfs (Sindelar & Jadrnicek, 1980) and to lie approximately 500–600 m below the sediment/water interface beneath the upper slope. The presence of the Miocene gypsum in the eastern Mediterranean has been well documented as acting as a weak plastic stratum in the deformation of the Mediterranean Ridge (Smith, 1976; Stride et al., 1977; Kempler, Mart, Herut & McCoy, 1996; Chaumillon & Mascle, 1997) and the western Nile Cone (Kenyon, Belderson & Stride, 1975; Ross et al., 1978; Mart, 1993). Movement on a glide plain of Messinian evaporites is therefore believed to have been important in emplacement of the HBM.

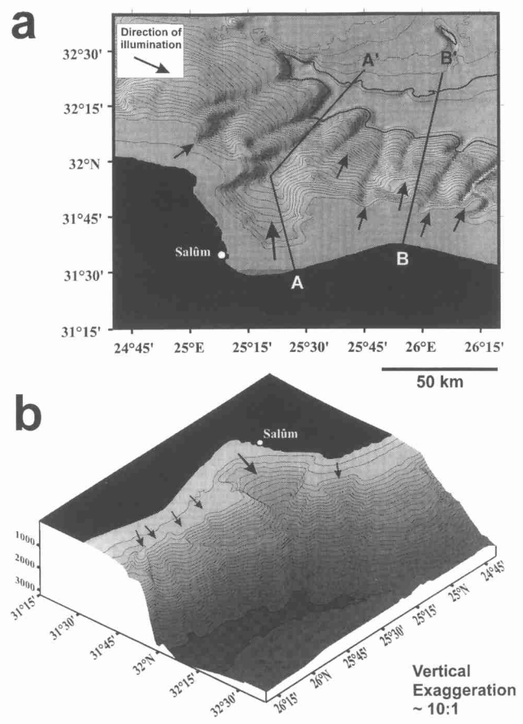

Fig. 9. Two views of the Gulf of Salûm, the postulated source area for the HBM, west of the Nile Delta (see Fig. 1 for location). Both show the SW margin of the Herodotus Basin (thicker contour line or dark shaded) and arrows delineating the major and minor canyons. Bathymetry from the GEBCO Digital Atlas (Jones, Tabor & Weatherall, 1994) with 100 m depth intervals. (a) Contoured plan view of the region showing shaded bathymetry with illumination from the WNW. Transects A-A′ and B-B′ are shown in Fig. 11b. (b) 3-D view of the NE African margin showing the 'funnel-shaped' Gulf of Salûm embayment. Approximate volume of embayment and associated canyon is 300 km^3. Smaller canyons on the Egyptian continental slope to the east of the Gulf are also visible and are suggested by Cita et al. (1984a) to be the main collapse and source region.

8.2. Trigger mechanism

Several mechanisms are known to act singly or together in the triggering of large volume slides, which can then evolve into very large turbidity currents (see summary in the Section 1). It is very difficult to determine which of these mechanisms was most important for any particular megaturbidte. We simply point out here some of the factors that seem most likely to have contributed to emplacement of the HBM some 27,000 years ago.

8.2.1. Low sea level

The date of the last glacial maximum (LGM) occurred at approximately 22 ka before present (CLIMAP, 1976). The 27.1 ka date obtained for the emplacement of the HBM corresponds to the lowering of sea-level prior to the LGM, (Fig. 10) and represents one of the first megaturbidites to be dated absolutely and correlated to a sea level·regression. During this time eustatic sea-level lowered at a rate of between 4 and 8 m/ka reaching a low stand at approximately 75–100 m below present day level (cf Shackleton, 1987), thus exposing a large part of the north African shelf. This in turn would have decreased the pore pressure in the sediments by approximately 760 kbars (using Pressure = $h\rho g$, where 'h' is the height of the water column removed [75 m], 'ρ' is the density of that water [1030 kg/m^3] and 'g' is the acceleration due to gravity [9.81 m/s]), thereby removing water load acting on the weak stratigraphic layer (evaporites) as well as lowering cohesion of shelf edge sediments.

8.2.2. Oversteepening of the shelf/slope

The present day NE African shelf and slope lie on a WNW–ESE trending extensional fault system that is down-faulted to the north. The development of these faults can be related to the Miocene opening of the Red Sea and the gradual subsidence and deformation of the eastern Mediterranean associated with the initial stages of Eurasian plate subduction by the African plate (Ross et al., 1978; Sestini, 1984). The fault network extends from the Al Jabal Al Akhdar uplift of northern Cyrenaica in the west to the Dead Sea Transform fault along the coasts of the Lebanon and Syria in the east (Röhlich, 1980). Offsets of these faults are visible in the coastline of the continental margin and are thought to be related to some dextral strike slip movement between these predominantly normal faults (Sestini, 1984). Middle to Late Miocene faulting led to a relatively steep continental slope with a narrow (15–50 km) shelf (Figs. 1, 9 and 11). The initial faulting led to uplift of the Al Jabal Al Akhdar region (Cyrenaica uplift, Goudarzi, 1980) with simultaneous subsidence of the Herodotus Basin and Herodotus Trough. The increased rate of convergence of the African and Eurasian tectonic plates in the Plio- Pleistocene led to further downfaulting of the continental margin and deepening of the Herodotus Basin and Trough (Sestini, 1984), such that the slope angle is now approximately 6°.

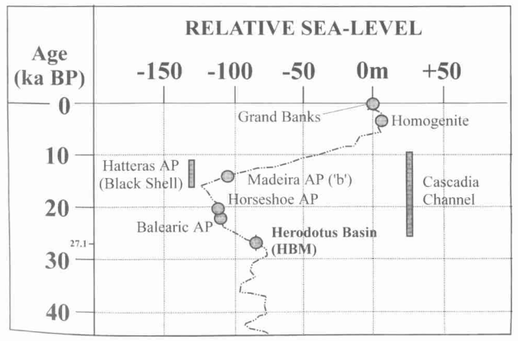

Fig. 10. Sea level curve during the late Pleistocene (after Shackleton, 1987) with the estimated date for the HBM (27.1 ka) plotted on the curve. Other megaturbidites discussed in the literature are also plotted showing the high frequency of reported megaturbidites during the low sea-level period between 10–30 ka.

8.2.3. Seismic activity

The historical record of earthquake activity in the SE Mediterranean shows that activity is located in five main regions (Papazachos 1973; Kebeasy 1980, 1990). These are: (1) the major tectonic plate intersections (Eurasian, African, Arabian and Aegean microplate); (2) along the Mediterranean Ridge accretionary prism; (3) within the sediments of the Nile Delta and Nile Fan; (4) on the continental margin, related to the belt of Neogene down-faulting; and (5) the Red Sea rift. The larger magnitude shocks (between 6.5 and 8 RS) are commonly located on the Mediterranean Ridge and Nile Cone and Delta, (Papazachos, 1973; Kebeasy, 1980), but the largest earthquakes are associated with the Anatolian and Aegean microplate boundary earthquakes to the north and from the Red Sea rift to the east of the study region. Earthquakes located along the NE African continental margin occur at a high frequency, with one shock of M > 6.5 RS approximately every 10 years and lesser magnitude quakes approximately every 2 years (Papazachos, 1973). Clearly, this high frequency of seismic activity has the potential to destabilise the sediment and trigger a major slide event in the Gulf of Salûm.

8.2.4. Sediment oversupply

The HBM has a mixed composition that requires a supply of both carbonate and terrigenous material in approximately equal proportions. The terrigenous material is thought by Cita et al (1984a) to have been supplied preferentially by the anti-clockwise eastern

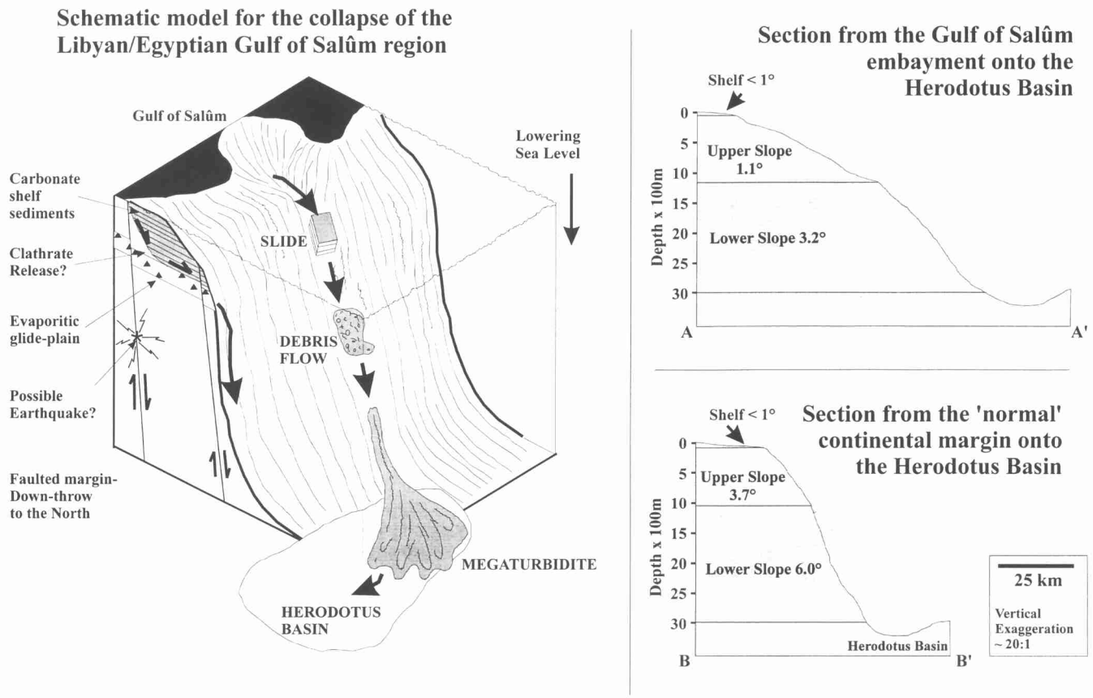

Fig. 11. (a) A schematic model for the emplacement of the HBM, showing the influencing physiographical features of the region during the late Quaternary. (b) A comparison between the upper and lower slopes of the Gulf of Salûm embayment and the 'normal' continental margin. The approximate 3° difference in the upper slopes of the two examples may be due to the removal of material from the Gulf of Salûm embayment as part of the 26.4 ka HBM event. Locations of sections are shown in Fig. 9a.

Mediterranean Gyre transporting material from a northern source. However, we note the signature of Nile-derived material in the HBM that suggests either alongshelf supply or, more likely, significant erosion of previously emplaced Nile Cone material by the HBM. The Gulf of Salûm would certainly be a possible location for rapid biogenic accumulation with its broad shallow shelf and the possible supply of nutrients from the Mediterranean Gyre. The measured 500–600 m of sediment above the Messinian evaporites would suggest an overall accumulation rate of approximately 8 cm/ka, over the past 6 Ma. Tectonic downfaulting of the upper slope in the Gulf of Salûm region may have given the extra accommodation space required for increased accumulation of carbonate material, creating an unstable sediment body.

8.2.5. Other factors

As a result of the loss of hydrostatic pressure any buried gas hydrates or clathrates may have degassed and decreased the pore pressure further. Large areas of accumulated clathrates in the eastern Mediterranean were proposed by Kvenvolden, Ginsburg and Soloviev (1993) and Miles (1995) on theoretical grounds, although little direct evidence exists as yet. Destabilisation of the margin by impact of a tsunami wave is considered less likely due to the very large volume of material that was redeposited and large area affected during the collapse.

Evolution of the continental shelf and upper slope off NE Africa, leading to the emplacement of the HBM is summarised in Fig. 11. Unfortunately, no data exist from the more proximal slope regions that might allow us to confirm the presence or passage of a major slide-debris flow event.

8.3. Megaturbidite concept

There have been relatively few detailed studies of megabeds or megaturbidites reported in the literature to date. Review of some of the best documented examples reveals some important differences between those described from ancient successions and those from modern basin plains (Table 7, Reeder et al., in prep.). Most of the ancient examples are very thick bedded (average 40 m) but relatively restricted areally

Table 7
Examples of the geometries from other documented megaturbidites, comprising six from both the ancient and recent geological record. The area over which the two separate groups of turbidites can be traced shows the greatest difference

Ancient megaturbidite	Location	Reference	Max. thickness (m)	Approx. area (km^2)	Approx. volume (km^3)
Ancient (>1 Ma)					
Gordo Megabed	Tabernas Basin, SE Spain	Kleverlaan (1987)	9	190	> 6
Petite Bar Calcaire	N. Pyrenean Basin, S France	Doyle and Bourrouilh (1986); Debroas, Lagier and Souquet (1983)	25	120	~ 3
Grand Bar Calcaire			63	1000	~ 60
Missaglia Megabed	Lombardian Basin, N Italy	Bernoulli et al. (1981)	30	250	~ 15
Roncal Unit	SW Pyrenean Foreland Basin, Spain	Rupke (1976); Johns et al. (1981); Labaume et al. (1987)	~ 50	900	~ 75
Dalmatian Flysch	Croatia	Marjanac, 1996	> 49	140	~ 42
Average			40	435	35
Recent (<1 Ma)					
Grand Banks turbidite	Sohm A.P., Newfoundland	Heezen and Ewing (1952)	3	70,000	185
Black Shell turbidite	Hatteras A.P., W Atlantic	Piper and Aksu (1987)	4.3	50,000	> 100
Horseshoe A.P Turbidite H13	Iberian Margin, E Atlantic	Lebreiro et al. (1997)	> 4.9	> 21,000	> 33
Balearic A. P. megabed	W Mediterranean	Rothwell et al. (1998)	10	< 60,000	450
HBM	SE Mediterranean	This study	> 16.26	40,000	400
Madeira A. P. Turbidite F	E. Atlantic margin	Rothwell et al. (1992)	5	64,000	190
Average			7	51,000	225

(average 435 km^2). We propose that these are better termed *composite megabeds* as they typically include thick, chaotic slide and debrite portions as well as graded turbidite tops. They probably represent the more proximal deposits resulting from large-scale margin collapse, that typically occur over a restricted area in a channel, slope or base-of-slope setting.

The modern examples are generally less thick bedded (average 7 m) but far more areally extensive (average 51,000 km^2), and hence also have very large total volumes. These are, perhaps, the more distal equivalents of composite megabeds in which only the turbidite portion remains to be spread out over even very large basin plains. We propose these as the megaturbidites *sensu stricto*.

Although it is important to distinguish megabeds from megaturbidites, particularly with regard to their different depositional processes, likely settings and lateral extent, we suggest there are insufficient data at this stage to allow any more rigorous definition by thickness, volume or other criteria (see also Bouma, 1987). The early definitions proposed by Ricci Lucchi and Valmori (1980) of >1 m thick or Mutti et al. (1984) of >1 km^3, are both rather small in light of recent work on modern examples. Furthermore, an important criterion for any *megaturbidite* should be its very large lateral extent.

9. Conclusions

The Herodotus Basin Megaturbidite represents the single major event in the sedimentary record of the Herodotus Basin during the past 30,000–40,000 years. It is a truly basinwide deposit with a maximum thickness of 18.6 m in the cores (at least 20 m from seismic evidence), a lateral extent of 400 × 100 km (40,000 km^2) and a volume of approximately 400 km^3 of mixed carbonate/terrigenous material. The most likely source of the original slide is the present funnel-shaped marginal embayment known as the Gulf of Salûm on the Libyan/Egyptian continental shelf/slope. Volumetric estimates of the amount of material removed to form this embayment correlate relatively well with those of the HBM, but suggest that additional material was supplied from another source.

The HBM shows a number of properties and processes that have not been described previously for megaturbidites anywhere. These distinctive characteristics, together with its basinwide extent, make the HBM an excellent marker bed in any stratigraphic reconstruction of the basin.

1. Whereas the composition of associated thin turbidites derived from the Libyan/Egyptian shelf ('Type-B') show a predominant carbonate source, those from the Nile Cone ('Type-A') are terrigenous in composition. The HBM has a composition somewhere between the two sources with a more terrigenous signature in the more distal regions. This is most likely due to erosion of the underlying Nile Cone-derived turbidites as the HBM turbidity current proceeded north-easterly along the basin plain. Indeed, Cita et al. (1984a) noted clear erosion at the base of the HBM from their study. Our volume estimates indicate that this erosion may have been up to 100 km^3 of material in total.
2. The HBM is seen to interact with the seafloor topography of the Herodotus Basin, both from seismic expression of the acoustically transparent layer and evidence from core data. The ATL is seen to onlap onto the small deformation ridges that parallel the Mediterranean Ridge (Fig. 3c) throughout the length of the basin and both grain size and sedimentary structures in core sections (Fig. 7c) show probable fluctuations in velocity of the flow, that might have resulted from topographic influence.
3. Sedimentary structures in the proximal part of the HBM are somewhat indistinct, commensurate with very rapid deposition. Distally, the structures are perhaps best described according to the Stow (1977) model for fine-grained turbidites (Stow & Piper, 1984), although each of the divisions is considerably expanded and evidence of repetition is common.

Several factors are believed to have conspired to cause the catastrophic collapse that led to emplacement of the HBM 27.1 ka before present. These include lowered sealevel and attendant sediment destabilisation, the presence of a weak horizon within the sediment pile to act as a glide plane, tectonic oversteepening of the upper slope and a probable seismic trigger. More detailed work is required to better characterise both modern and ancient megaturbidites before a strict definition can be agreed. We suggest here, however, that a distinction be made between composite (often tripartite) *megabeds* that are extremely thick but laterally restricted, and *megaturbidtes* that are both very thick and laterally very extensive.

Acknowledgements

Special thanks to the Officers, Crew and Shipboard Scientific Party of *Marion Dufresne* Cruise 81 and particularly to Yvon Balut and his coring team for their expert recovery of the cores. NERC Scientific Services, Radiocarbon Laboratory, East Kilbride is thanked for their support in obtaining the radiocarbon dates (^{14}C Dating Allocation No. 664/0896). Thanks also to NERC's British Ocean Sediment Core Repository (BOSCOR) based at the SOC where description and sampling was carried out. MSR acknowledges the help of Roger Urgeles (Barcelona University) and Paul Kelly (SOC) with analysis of bathymetric data. MSR's PhD is NERC funded GT4/95/288/E. This work was also supported by the European Union Marine Science and Technology Programme Contract No. MAS2-CT93-0051.

References

Amorosi, A., Colalongo, M. L., & Vaiani, S. C. (1996). Detecting a sequence boundary across different tectonic domains — an example from the middle Miocene of the northern Apennines (Italy). *Terra Nova*, *8*, 334–346.

Bard, E., Arnold, M., Fairbanks, R. G., & Hamelin, B. (1993). 23OTh-234U and 14C obtained by mass spectrometry on corals. *Radiocarbon*, *35*, 191–199.

Bernoulli, D., Bichsel, M., Bolli, H. M., Haring, M. O., Hochuli, P. A., & Kleboth, P. (1981). The Missaglia Megabed, a catastrophic deposit in the Upper Cretaceous Bergamo Flysch, northern Italy. *Eclogae Geologicae Helvetiae*, *74*, 421–442.

Bouma, A. H. (1962). *Sedimentology of some flysch deposits: A graphic approach to facies interpretation*. Amsterdam: Elsevier 168 pp.

Bouma, A. H. (1987). Megaturbidite: an acceptable term? *Geo-Marine Letters*, *7*, 63–67.

Bugge, T., Befring, S., Belderson, R. H., Eidvun, T., Jansen, E., Kenyon, N. H., Holtedahl, H., & Seirup, H. (1987). A giant three-stage submarine slide off Norway. *Geo-Marine Letters*, *7*, 191–198.

Chaumillon, E., & Mascle, J. (1997). From foreland to forearc domains: new multichannel seismic reflection survey of the Mediterranean ridge accretionary complex (eastern Mediterranean). *Marine Geology*, *138*, 237–259.

Chough, S. K., Hwang, I. G., & Choe, M. Y. (1990). The Miocene Doumsan fan-delta, SE Korea: a composite fan-delta system in a back arc margin. *Journal of Sedimentary Petrology*, *60*, 445–455.

Cita, M. B., Beghi, C., Camerlenghi, A., Kastens, K. A., McCoy, F. W., Nosetto, A., Parisi, E., Scolari, F., & Tomadin, L. (1984a). Turbidites and Megaturbidites from the Herodotus Abyssal Plain (eastern Mediterranean) unrelated to seismic events. *Marine Geology*, *55*, 79–101.

Cita, M. B., Camerlenghi, A., Kastens, K. A., & McCoy, F. W. (1984b). New findings of the Bronze age Homogenites in the Ionian Sea: geodynamic implications for the Mediterranean. *Marine Geology*, *55*, 47–62.

Cita, M. B., Camerlenghi, A., & Rimoldi, B. (1996). Deep sea tsunami deposits in the eastern Mediterranean: new evidence and depositional models. *Sedimentary Geology*, *104*, 155–173.

CLIMAP project members (1976). The surface of ice age earth. *Science*, *191*, 1131–1137.

Debroas, E. J., Lagier, Y., & Souquet, P. (1983). Carbonate megabeds in the Turonian-Coniacian turbidites of the North-Pyrenean Flysch (Northwestern Pyrenees, France). *Bulletin de la Society Geologique de France*, *25*, 911–919.

Doyle, L. J., & Bourrouilh, R. (1986). Carbonate megaturbidites — examples from the Gulf of Mexico and the French Pyrenees. *American Association of Petroleum Geologists Bulletin*, *70*, 583.

Elmore, R. D., Pilkey, O. H., Cleary, W. J., Curran, W. J., & Curran, H. A. (1979). Black Shell turbidite, Hatteras Abyssal Plain, western Atlantic Ocean. *Geological Society America Bulletin*, *90*, 1165–1176.

Evans, D., King, E. L., Kenyon, N. H., Brett, C., & Wallis, D. (1996). Evidence for long-term instability in the Storegga Slides region off western Norway. *Marine Geology*, *130*, 281–292.

Goudarzi, G. H. (1980). Structure — Libya. In M. J. Salem, & M. T. Busrewil, *The geology of Libya, vol. III* (pp. 879–892). London: Academic Press Inc.

Grant, J. A. (1986). The Isocon Diagram — a simple solution to Gresens' Equation of Metasomatic alteration. *Economic Geology*, *81*, 1976–1982.

Heezen, B. C., & Ewing, M. (1952). Turbidity currents and submarine slumps, and the 1929 Grand Banks earthquake. *American Journal of Science*, *250*, 849–873.

Heike, W. (1984). A thick Holocene Homogenite from the Ionian Abyssal Plain (eastern Mediterranean). *Marine Geology*, *55*, 63–78.

Iturralde-Vinent, M. A. (1992). A short note on the Cuban late Maastrichtian megaturbidite (an impact-derived deposit?). *Earth and Planetary Science Letters*, *109*, 225–228.

Johns, D. R., Mutti, E., Rosell, J., & Seguret, M. (1981). Origin of a thick redeposited carbonate bed in Eocene turbidites of the Hecho Group, south-central Pyrenees, Spain. *Geology*, *9*, 161–164.

Jones, M. T., Tabor, A. R., & Weatherall, P. (1994). *GEBCO digital atlas (CD ROM and 3.5″* Disks, version 1.06). Bidston, CD: British Oceanographic Data Centre Publishing 70 pp.

Kahler, G., & Dossi, M. (1996). Micropalaeontology. In R. G. Rothwell, R/V *Marion Dufresne Cruise 81 — Mediterranean giant piston coring transect*, Cruise Report, 40–63. (Unpublished manuscript).

Kebeasy, R. M. (1980). Seismicity and seismotectonics of Libya. In M. J. Salem, & M. T. Busrewil, *The geology of Libya, vol. III* (pp. 955–963). London: Academic Press Inc.

Kebeasy, R. M. (1990). Seismicity. In R. Said, *The geology of Egypt* (pp. 51–59). Rotterdam: A. A. Balkema Publishers.

Kempler, D., Mart, Y., Herut, B., & McCoy, F. W. (1996). Diapiric features in the southeastern Mediterranean Sea: possible indication of extension in a zone of incipient continental collision. *Marine Geology*, *134*, 237–248.

Kenyon, N. H., Belderson, R. H., & Stride, A. H. (1975). Plan views of active faults and other features on the Lower Nile Cone. *Geological Society of America Bulletin*, *86*, 1733–1739.

Kleverlaan, K. (1987). Gordo Megabed: a possible seismite in a Tortonian submarine fan, Tabernas Basin, Province Almeria, south-east Spain. *Sedimentary Geology*, *51*, 165–180.

Kvenvolden, K. A., Ginsburg, G. A., & Soloviev, V. A. (1993). Worldwide distribution of subaquatic gas hydrates. *Geo-Marine Letters*, *13*, 32–40.

Labaume, P., Mutti, E., Seguret, M., & Rosell, J. (1983). Carbonate megaturbidites of the South-Pyrenean lower and middle Eocene turbiditic basin. *Bulletin de la Society Geologique de France*, *25*, 927–941.

Labaume, P., Mutti, E., & Seguret, M. (1987). Megaturbidites: A depositional model for the Eocene of the SW-Pyrenean foreland basin, Spain. *Geo-Marine Letters*, *7*, 91–101.

Lebreiro, S. M., McCave, I. N., & Weaver, P. P. E. (1997). Late Quaternary turbidite emplacement on the Horseshoe abyssal plain (Iberian margin). *Journal of Sedimentary Research*, *67*, 856–870.

Lucchi, R., & Camerlenghi, A. (1993). Upslope turbiditic sedimentation on the southeastern flank of the Mediterranean ridge. *Bollettino di Oceanologia Teorica ed Applicata*, *11*, 3–25.

Marjanac, T. (1996). Deposition of megabeds (megaturbidites) and sea-level change in a proximal part of the Eocene-Miocene flysch of central Dalmatia (Croatia). *Geology*, *24*, 543–546.

Mart, Y. (1993). The sedimentologic and geomorphic provinces of the Nile Fan. In E. G. Rhodes, & T. S. Moslow, *Marine clastic reservoirs* (pp. 101–112). New York: Springer-Verlag.

Miles, P. R. (1995). Potential distribution of methane hydrate